Communication

Sub-60-fs, 1300-nm Laser Pulses Generation from Soliton Self-Frequency Shift Pumped by a Femtosecond Yb-Doped Fiber Laser

Hongyuan Xuan , Kong Gao * , Xingyang Zou , Ze Zhang , Wenchao Qiao * , Yizhou Liu

Posted Date: 17 July 2025

doi: 10.20944/preprints202507.1425.v1

Keywords: sub-hundred femtosecond 1300-nm laser; soliton self-frequency shift; Yb-doped femtosecond fiber laser; high nonlinearity photonic crystal fiber

 doi:10.20944/preprints202507.1425.v1

Communication

Sub-60-fs, 1300-nm Laser Pulses Generation from Soliton Self-Frequency Shift Pumped by a Femtosecond Yb-Doped Fiber Laser

Hongyuan Xuan [1], Kong Gao [1,*], Xingyang Zou [1], Ze Zhang [1], Wenchao Qiao [1,2,*] and Yizhou Liu [1,2]

[1] School of Information Science and Engineering, Shandong University, Qingdao 266237, China

[2] Key Laboratory of Laser & Infrared System, Ministry of Education, Shandong University, Qingdao 266237, China

* Correspondence: gaokong@sdu.edu.cn (K.G.); wenchao.qiao@sdu.edu.cn (W.Q.)

Abstract

We report on the generation of 1300-nm ultrashort laser pulses via the soliton self-frequency shift in a high-nonlinearity fiber, pumped by the 41.9-MHz, 67.9-fs, 1073-nm femtosecond laser emitted from an Yb-doped fiber laser system. A numerical simulation was applied to investigate the spectral broadening process driven by the soliton self-frequency shift with increased pump power. The experimental results are in good agreement with the numerical results, delivering a 33-mW, 57.8-fs 1300-nm Raman soliton filtered by a longpass filter. The impact of the polarization direction of the injected pump laser on the soliton self-frequency shift process was also further investigated. The root means squares of the the Yb-doped fiber laser and the nonlinearly spectral broadened laser were 0.19%@1h and 0.23%@1h, respectively.

Keywords: sub-hundred femtosecond 1300-nm laser; soliton self-frequency shift; Yb-doped femtosecond fiber laser; high nonlinearity photonic crystal fiber

1. Introduction

Ultrafast laser sources with central wavelength located at 1300-nm make great contributions in the field of three-photon microscopy (3PM), especially for deep tissue imaging such as deep brain imaging in freely behaving rodents [1–5]. Utilizing the high-energy, 1300-nm femtosecond pulse as the illumination source for the 3PM allows for deep penetration depth (>1 mm) with high signal-to-background contrast and negligible out-of-focus fluorescence [1–5]. A. Klioutchnikov et al. reported a head-mounted three-photon microscope (3PM) for imaging deep cortical layer neuronal activity in a freely moving rat by using a 55.7-fs, 200-nJ, 1320-nm ultrafast laser source, enabling an imaging depth of >1.1 mm below the cortical surface [1]. C. Zhao et al. demonstrated a miniatured 3PM to maximize fluorescence collection by using a <100-fs, 126-nJ, 1300-nm laser source, which was capable of imaging calcium activity throughout the entire cortex and dorsal hippocampal CA1 with the imaging depth up to 1.2 mm [2].

High-energy, ultrafast 1300-nm illumination source for the 3PM can be realized with the optical parametric amplification (OPA) process [6,7], delivering the 1300-nm laser as the amplified idler laser with the signal laser realized by white-light generation. However, the potential long-term instability of the white-light generation process and the potential spatial chirp of the amplified idler laser during the OPA process seriously affect the operational performance of the 3PM. Directly utilizing the 1300-nm sub-hundred femtosecond laser as the seed laser for the OPA process is an ideal approach in realizing high-energy, ultrafast 1300-nm laser source with better long-term systematic stability and significantly inhibited spatial chirp [8].

 doi:10.20944/preprints202507.1425.v1

Nowadays, the 1300-nm femtosecond seed laser can be generated directly either from the mode-locked fiber lasers [9–13] or nonlinear frequency conversion systems [14–16]. Bismuth-doped (Bi-doped) fibers are reported to be the appropriate gain medium in generating the 1300-nm mode-locked laser pulses [9,10]. However, the relatively low small-signal gain of ~0.12 dB/m at 1.32 μm seriously restricts its further applications in generating sub-hundred femtosecond seed laser [9,17]. The nonlinear frequency conversion based on the self-phase modulation (SPM), or the Raman soliton self-frequency shift (SSFS) can be utilized in generating the sub-hundred femtosecond 1300-nm seed lasers [14–16]. H. Chung achieved the 97-fs, 15.8-nJ, 1300-nm laser pulses employing on the SPM effect, after propagating the 290-fs, 160-nJ, 1560-nm laser through the dispersion-shifted fiber [14]. No further amplification results realized by the OPA process were reported, limited by the power scaling capability of the reported 1560-nm fiber laser source.

The SSFS driven by the stimulated Raman scattering (SRS) in a negative dispersion region at 1 μm can be utilized to generate the sub-hundred femtosecond 1300-nm laser pulses, which has been realized with the large mode area (LMA) fiber and the noble gas-filled hollow-core fiber. L. Rishøj et al. reported the generation of 30-nJ, 120-kHz, 53.6-fs, 1317-nm femtosecond laser in a LMA fiber with an effective mode area of 660 μm^2 [18]. Due to the LMA property of the fiber, the transverse mode of the generated 1317-nm laser was LP_{09}, which requires extra optical beam conversion construction to reconvert the beam back to the Gaussian-like beam. Y. Eisenberg et al. realized the 500-nJ, 200-kHz, 80-fs, 1310-nm ultrafast laser in a hollow-core fiber filled with N_2 gas [19]. However, the utilized hollow-core fiber with 30-μm core diameter can also introduce transverse mode problems with increased systematic complexity and higher costs [20]. In comparison, based on the development of the photonic crystal fiber (PCF), the single-mode (SM) 1300-nm Raman soliton laser with sub-hundred femtosecond pulse duration can be generated with much simple and robust systematic construction by utilizing the high nonlinearity PCF (HNPCF). Based on the modified air-holes of the cladding, the waveguide properties of the HNPCF, such as dispersion, transverse mode and mode field diameter can be carefully designed by adjusting the air-hole diameter and the distance between the adjacent air-holes. Typically, the zero dispersion of the pure silica fiber can be shifted from ~1310 nm to ~1040 nm, with the mode field diameter decreased to ~4 μm [21]. These properties enable the generation of the sub-hundred femtosecond, SM 1300-nm soliton laser with the SSFS process, pumped by a femtosecond Yb-doped fiber laser with high power-scaling capability. Further, the input polarization can also be optimized to ensure the optical power mainly distributed inside the fundamental Raman soliton before and after the Raman soliton contents shifting to 1300 nm. Therefore, an ideal 1300-nm Raman soliton seed laser can be generated with promising optical power for the OPA process, fulfilling the urgent requirements of the 3PM applications. To the best of our knowledge, such kind of 1300-nm seed laser generation system has not been reported yet.

In this paper, we report the generation of the 33-mW, 57.8-fs, 1300-nm seed laser, realized with the SSFS process pumped by a 136-mW, 67.9-fs, 1073-nm femtosecond Yb-doped fiber laser. Numerical simulation based on solving the nonlinear Schrödinger equation was conducted to predict the spectral evolution under different injected pump power in the HNPCF. Further experiment achieved the 33-mW, 57.8-fs, 1300-nm femtosecond laser with high pulse quality. Study on the impact of the polarization direction of the pump laser on the SSFS process was also investigated, indicating a polarization-dependent SSFS process. The output power stabilities of the Yb-doped fiber amplifier and the spectral broadened laser were measured with root mean squares (RMS) of 0.19%@1h and 0.23%@1h, respectively.

2. Experimental Setup

The schematic construction of the 1300-nm femtosecond laser system is shown in Figure 1. The system consists of a polarization-maintaining (PM) mode-locking Yb-doped fiber oscillator, a PM SM Yb-doped fiber pre-amplifier, a grating-pair pre-chirper, a PM double-cladding (DC) Yb-doped fiber power amplifier, a grating-pair compressor and a SSFS stage. The home-built PM mode-locking Yb-doped fiber oscillator based on the nonlinear amplifying loop mirror (NALM) consists of a nonlinear

 doi:10.20944/preprints202507.1425.v1

loop, a reflection linear arm, and a transmission port. A PM fiber coupler with a power splitting ratio of 45:55 was utilized to connect the nonlinear loop with the linear arm and the transmission port. About 50-cm PM Yb-doped fiber (Yb401-PM, INO) was utilized in the nonlinear loop as the gain medium, pumped with a SM 976-nm laser diode (LD) through a PM fiber WDM. A PM fiber phase bias with a phase shift of -π/2 was included in the nonlinear loop to ensure the self-starting mode-locking. The linear arm consists of a bandpass spectral filter (FLH1030-10, Thorlabs) for spectral management and a transmission grating pair (T-1000-1040, LightSmyth) for intracavity dispersion management.

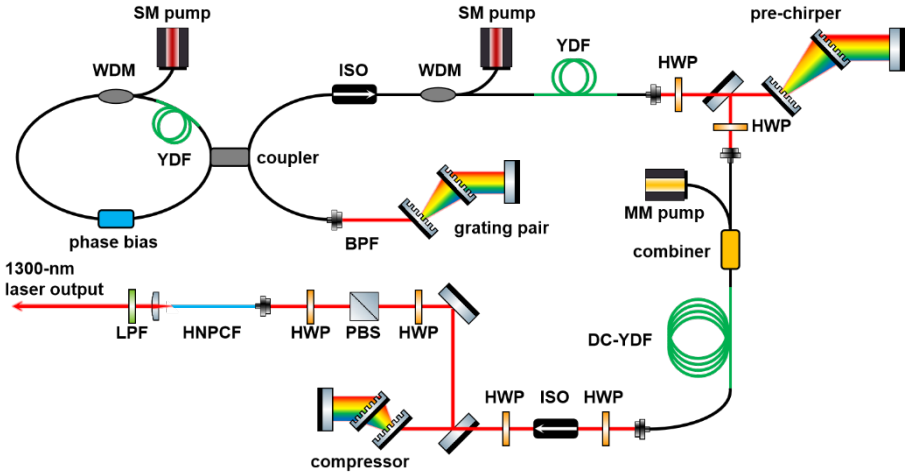

Figure 1. Schematic construction of the 1300-nm femtosecond laser system. WDM: wavelength division multiplexer, YDF: Ytterbium-doped fiber, BPF: bandpass filter, ISO: isolator, HWP: half-wave plate, DC: double-cladding, PBS: polarizing beam splitter. HNPCF: high nonlinearity photonics crystal fiber, LPF: longpass filter, MM: multi-mode.

The mode-locked laser pulses output from the fiber oscillator were delivered from the transmission port and subsequently injected into the PM fiber pre-amplifier. The PM fiber pre-amplifier consists of a PM WDM, a SM 976-nm LD, and an about 50-cm Yb-doped fiber (Yb401-PM, INO). The pre-amplified mode-locking laser pulses were then modulated with a transmission grating-pair pre-chirper which provided negative group velocity dispersion. After that, the mode-locking laser pulses were coupled into the fiber power amplifier composed of a 976-nm multi-mode (MM) LD, a PM fiber combiner, a PM Yb-doped fiber (PM-YDF-5/130, Coherent) and a PM fiber collimator. The amplified laser pulses were then compressed by a transmission grating-pair compressor.

The compressed laser pulses were coupled from free space into an about 7.5-cm HNPCF (SC-5.0-1040-PM, NKT photonics) to pump the SSFS process. The input pump power was controlled with a variable attenuator consisting of a half-wave plate (HWP) and a polarizing beam splitter (PBS). The polarization direction of the input pump laser can be controlled with the HWP before the HNPCF. The output optical spectrum can be shifted to 1300 nm with the SSFS process. Finally, a longpass spectral filter (LPF, FELH1250, Thorlabs) was utilized to filter out the sub-hundred femtosecond 1300-nm laser pulses.

3. Experimental and Numerical Results

The NALM fiber oscillator operated in a dispersion-managed regime, delivering 1 mW, 41.9 MHz mode-locking laser pulses with a pulse to pulse interval of 23.87 ns, shown in Figure 2b. The optical spectrum of the mode-locking laser pulses is illustrated in Figure 2a, corresponding to a central wavelength of 1030 nm and a 3-dB spectral bandwidth of 16.6 nm. The average power of the mode-locked laser pulses was boosted to 52 mW by the PM fiber pre-amplifier. The pre-chirper provided a negative dispersion of -0.517 ps^2 at 1030 nm, enhancing the nonlinear spectral broadening

 doi:10.20944/preprints202507.1425.v1

process in the subsequent nonlinear fiber power amplifier. About 7-m PM DC Yb-doped fiber was utilized inside the fiber power amplifier, ensuring the gain managed nonlinear amplification process can be realized [22]. The optical spectrum of the amplified laser pulses was broadened to 54.3 nm with the central wavelength shifted to 1072.7 nm, as illustrated in Figure 2c. During the nonlinear amplification process, the SPM introduces linear chirp to the propagating laser pulses. Therefore, the amplified laser pulses can be compressed to the nearly transform limited pulse duration of 67.9 fs, which is 1.48 times the Fourier transform limited pulse duration. The corresponding auto-correlation trace is exhibited in Figure 2d, the residual pedestal may be attributed to uncompensated high-order dispersion. The optical average power of the compressed laser pulses was 407 mW, corresponding to an optical compression efficiency of ~80% and a polarization extinction ratio of 21.7 dB.

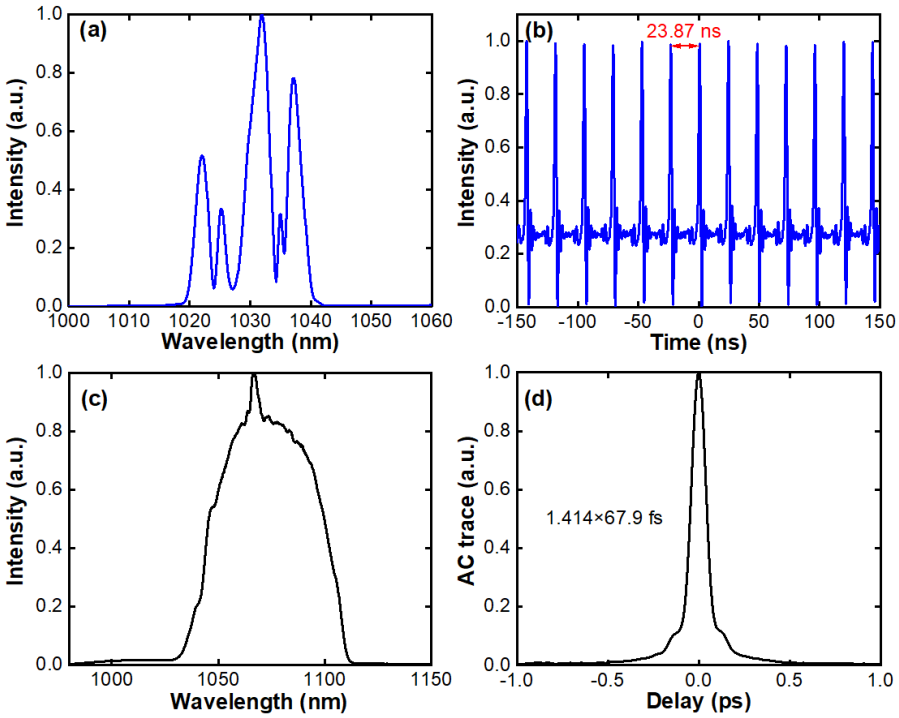

Figure 2. (a) Optical spectrum and (b) pulse train of the mode-locking laser pulses output from the transmission port, (c) optical spectrum and (d) auto-correlation trace of the compressed laser pulses output from the PM fiber power amplifier.

Figure 3 illustrates the dispersion curve of the HNPCF obtained from the NKT photonics. The corresponding photograph of the cross section is shown as the inset. The zero-dispersion wavelength is located at ~1040 nm, indicating a negative group velocity dispersion region with the optical wavelength above 1040 nm. The nonlinearity coefficient of the HNPCF is 11 $(W \cdot km)^{-1}$@1060 nm with the mode-field diameter of 4 μm. Based on the aforementioned optical characteristics, a numerical model was implemented to simulate the SSFS process with the 1072.7-nm pump laser propagating through the 7.5-cm PCF. The numerical model was built by solving the generalized nonlinear Schrödinger equation with the split-step algorithm [23,24]. The experimentally measured optical parameters of the 1072.7-nm pump laser were directly employed as the input parameters for the numerical simulation. The optical dispersion, SPM, SRS and the self-steepening effects in the fiber were included for the numerical simulation.

 doi:10.20944/preprints202507.1425.v1

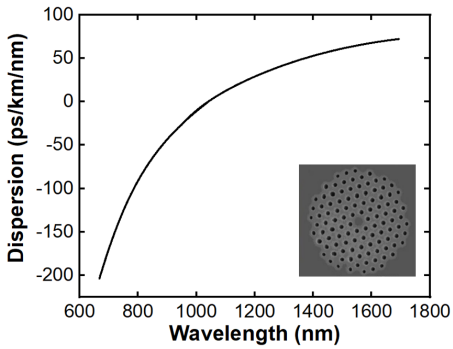

Figure 3. Dispersion parameter of the HNPCF under different wavelength, inset shows the scanning electron micrograph of the cross section of the HNPCF.

The numerical simulated optical spectral evolution of the 1072.7-nm pump laser propagating through the 7.5-cm HNPCF with different average power is illustrated in Figure 4. Figure 4a depicts the 2-Dimensional optical spectral evolution with increased pump power. Pure SPM dominated spectral broadening process can be observed with the injected 1072.7-nm pump power lower than 14 mW. The first-order Raman spectral contents were generated under the pump power of 19 mW, while the optical power located in the spectral range of 1050-1106 nm was clearly transferred to the Raman spectral contents. With the injected pump power increasing to 136 mW, the Raman spectral contents transformed to the Raman soliton and shifted from 1113 nm to 1300 nm with the anomalous group velocity dispersion of the HNPCF. The corresponding dispersive wave was also generated around 750 nm, locating in the normal group velocity dispersion region. Further higher-order Raman spectral contents can be also generated with higher injected pump power, shown in Figure 4a and Figure 4b. The calculated average power of the filtered 1300-nm Raman soliton is 32.5 mW. The calculated pulse duration of the corresponding transform limited auto-correlation trace is 66.2 fs, based on the $Sech^2$ assumption.

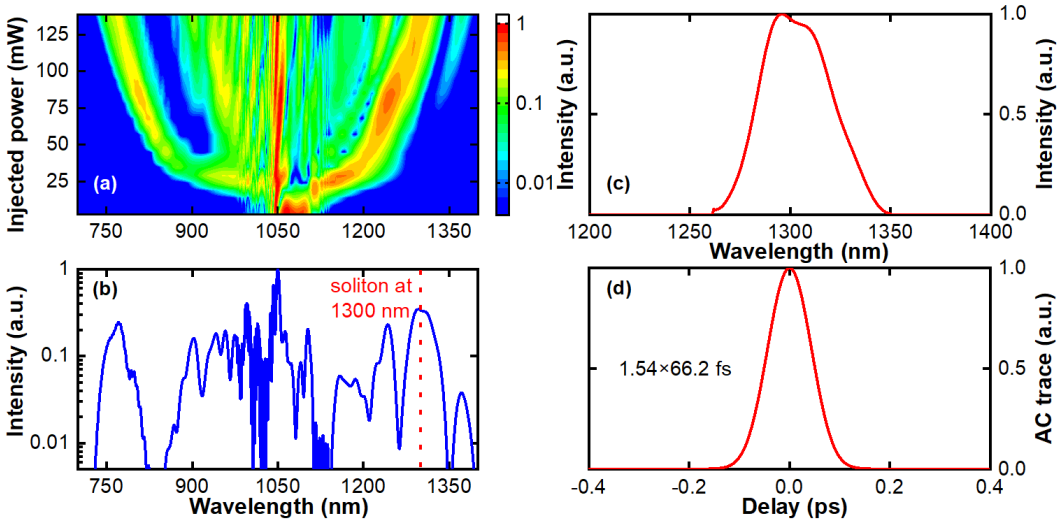

Figure 4. Numerical simulated (a) output spectra under different injected pump power, and (b) output spectrum under pump power of 136 mW, (c) optical spectrum and (d) transform-limited auto-correlation trace of the filtered 1300-nm soliton laser.

Based on the numerical results, the SSFS process was experimentally investigated with the linearly polarized pump laser propagating in the HNPCF. The output optical spectral evolution under different input pump power is illustrated in Figure 5a, which is highly consistent with the numerical results. The SPM dominated spectral broadening process under the pump power of 19 mW can be observed. Further increasing the pump power can result in the formation and frequency shift of Raman soliton in the negative group velocity dispersion region, along with the dispersive wave in

 doi:10.20944/preprints202507.1425.v1

the normal group velocity dispersion region. The measured output spectrum under the pump power of 136 mW is depicted in Figure 5b. The reddest Raman soliton component was successfully shifted to 1300 nm, which can be separated from the broadened optical spectrum with the LPF. Figure 5c shows the optical spectrum of the filtered 1300-nm soliton laser pulses, centered at ~1300 nm with a 3-dB spectral bandwidth of 46.6 nm. The corresponding auto-correlation trace is shown in Figure 5d, indicating a pulse duration of 57.8 fs based on the Sech² assumption, which is 1.38 times that of the Fourier transform limited pulse duration. The optical power of the sub-hundred femtosecond 1300-nm soliton laser was 33 mW, indicating a nonlinear frequency conversion efficiency of 24.3%.

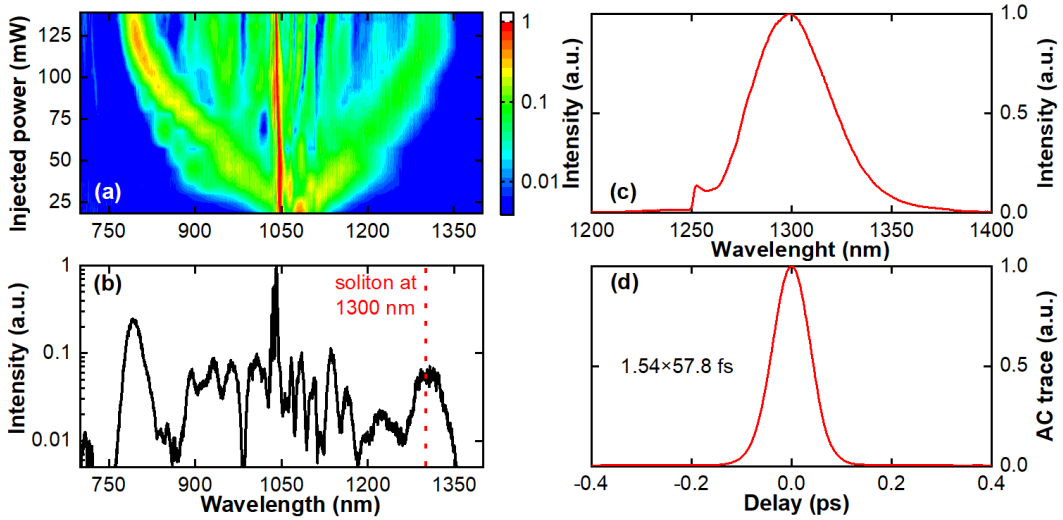

Figure 5. Experimental (a) output spectrum under different injected pump power, and (b) output spectrum under pump power of 136 mW, (c) optical spectrum and (d) auto-correlation trace of the 1300-nm soliton laser.

The impact of the input polarization on the SSFS process was further investigated with incrementally rotating the input polarization direction of the pump laser. The generated broadened 2-Dimensional optical spectra under the pump power of 136 mW is depicted in Figure 6. The Raman scattering induced SSFS process in the negative group velocity dispersion region was evidently affected with rotating the polarization direction of the input pump laser. The broadest nonlinear spectral broadening process induced by the SSFS can be realized with the polarization direction of the linearly polarized input pump laser rotated to be parallel with the optical axes of the HNPCF. Shown in Figure 6, with the generated 750-nm dispersive wave, the broadest nonlinearly broadened spectra can be achieved with the HWP rotation angle of 38.7°, 83.7°, 128.7°, 173.7°, 218.7°, 263.7°, 308.7°, and 353.7°, periodically increased with the rotation angle of 45°. The realized broadest nonlinearly broadened spectrum matches with the simulated results shown in Figure 4a well, indicating a perfect numerical model and reliable simulation results. Further modifying the input polarization direction can lead to the input pump laser decomposed into two orthogonal polarized optical components propagating through the fast axis and slow axis of the HNPCF. Therefore, the nonlinear spectral broadening process can be inhibited with the initial coupled pump power distributed into these two orthogonal polarized laser components, which can be further utilized to suppress the generation of high-order Raman solitons and concentrate more optical power in the fundamental Raman soliton. The narrowest spectral broadening results were achieved with the HWP rotation angle of 14.5°, 59.5°, 104.5°, 149.5°, 194.5°, 239.5°, 284.5°, and 329.5° periodically increased with the rotation angle of 45°. The cross-phase modulation was also introduced into the nonlinear spectral broadening process, lead to the further modulated spectral structures. Based on the aforementioned investigations, the HWP rotation angle was finally tuned to be 150° to modify the input polarization direction of the 136-mW pump laser to generate the 33-mW, 57.8-fs, 1300-nm seed laser for the OPA, shown in Figure 5.

 doi:10.20944/preprints202507.1425.v1

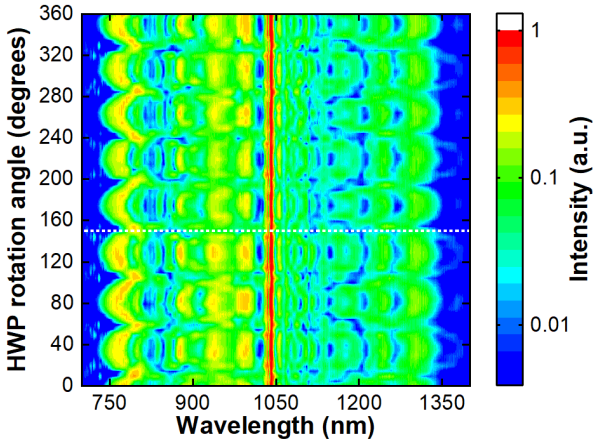

Figure 6. Evolution of the output optical spectrum under different polarization direction of the input pump laser.

To evaluate the stability of this system, the average power stabilities within 1 hour of the laser pulses output from the Yb-doped fiber laser and the HNPCF are both shown in Figure 7, of which the root mean squared (RMS) stability are 0.19%@1h and 0.23%@1h, respectively, indicating a high stability of the fiber laser system.

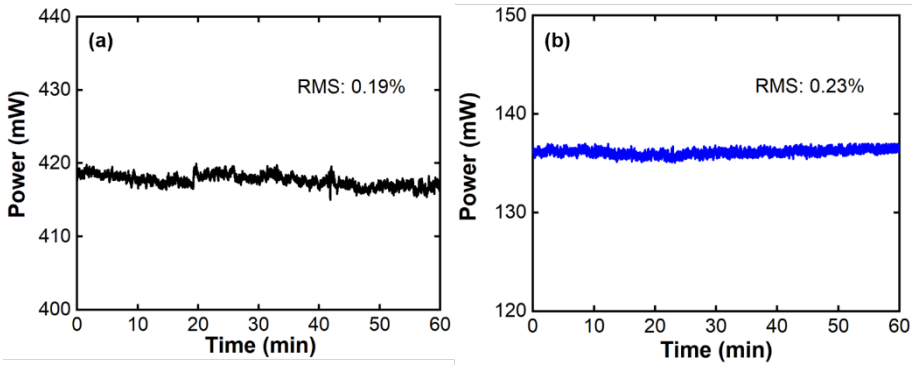

Figure 7. The average power stability of (a) the Yb-doped fiber laser and (b) the output laser from the HNPCF.

4. Conclusions

In conclusion, a 33-mW, 57.8-fs, 1300-nm femtosecond laser was realized through SSFS in a HNPCF pumped by an Yb-doped fiber laser. The Yb-doped fiber laser can deliver 41.9-MHz, 67.9-fs, 1072.7-nm femtosecond laser pulses with the maximum average power of 407 mW, with the RMS power stability within 1 hour of 0.19%. The spectral evolution of the 1-μm pump laser in the HNPCF under different input power was investigated with numerical simulation and experiments. The nonlinearly broadened spectrum perfectly covered the 1300-nm soliton waveband under the input pump power of 136 mW, with the RMS power stability within 1 hour of 0.23%. This work provides an ideal sub-hundred femtosecond 1300-nm seed laser for the OPA source of the 3PM applications [25].

Author Contributions: Conceptualization, H.X. and W.Q.; methodology, W.Q.; software, H.X.; validation, H.X., K.G., X.Z. and Z.Z.; investigation, H.X. and K. G.; resources, Y.L.; data curation, H.X.; writing—original draft preparation, H.X.; writing—review and editing, K.G., W.Q. and Y. L.; visualization, H.X.; supervision, K.G., W.Q. and Y.L.; All authors have read and agreed to the published version of the manuscript.

Funding: This research was funded by the National Natural Science Foundation of China, grant numbers 62305186, 62405164; National Key Research and Development Program of China, grant number 2024YFB4608901; and Natural Science Foundation of Shandong Province, grant number ZR2024QF206.

 doi:10.20944/preprints202507.1425.v1

Institutional Review Board Statement: No applicable.

Informed Consent Statement: No applicable.

Data Availability Statement: Date underlying the results presented in this paper are not publicly available at this time but may be obtained from the authors upon reasonable request.

Conflicts of Interest: The authors declare no conflicts of interest.

References

1. Klioutchnikov, A.; Wallace, D. J.; Frosz, M. H.; Zeltner, R.; Sawinski, J.; Pawlak, V.; Voit, K.; Russell, P. S. J.; Kerr, J. N. D. Three-photon head-mounted microscope for imaging deep cortical layers in freely moving rats. *Nat Methods* **2020**, *17*, 509-513.
2. Zhao, C.; Chen, S.; Zhang, L.; Zhang, D.; Wu, R.; Hu, Y.; Zeng, F.; Li, Y.; Wu, D.; Yu, F.; Zhang, Y.; Zhang, J.; Chen, L.; Wang, A.; Cheng, H. Miniature three-photon microscopy maximized for scattered fluorescence collection. *Nat Methods* **2023**, *20*, 617-622.
3. Streich, L.; Boffi, J. C.; Wang, L.; Alhalaseh, K.; Barbieri, M.; Rehm, R.; Deivasigamani, S.; Gross, C. T.; Agarwal, A.; Prevedel, R. High-resolution structural and functional deep brain imaging using adaptive optics three-photon microscopy. *Nat Methods* **2021**, *18*, 1253-1258.
4. Choe, K.; Hontani, Y.; Wang, T.; Hebert, E.; Ouzounov, D. G.; Lai, K.; Singh, A.; Béguelin, W.; Melnick, . M.; Xu, C. Intravital three-photon microscopy allows visualization over the entire depth of mouse lymph nodes. *Nat Immunol* **2022**, *23*, 330-340.
5. Ouzounov, D. G.; Wang, T.; Wang, M.; Feng, D. D.; Horton, N. G.; Cruz-Hernández, J. C.; Cheng, Y.; Reimer, J.; Tolias, A. S.; Nishimura, N.; Xu, C. In vivo three-photon imaging of activity of GCaMP6-labeled neurons deep in intact mouse brain. *Nat Methods* **2017**,*14*, 388-390.
6. Schulz, M.; Braatz, T.; Zapolnova, E.; Buß, J. H.; Golz, T.; Indorf, G.; Hofmann, L.; Grguraš, I.; Riedel, R. High power OPCPA system for in-vivo 2- and 3-photon brain imaging. SPIE BIOS, online, USA, 5 March 2021.
7. Guesmi, K.; Abdeladim,L.; Tozer, S.; Mahou, P.; Kumamoto, T.; Jurkus, K.; Rigaud, P.; Loulier,K.; Dray, N.; Georges, P.; Hanna,M.; Livet, J.; Supatto, W.; Beaurepaire, E.; Druon, F. Dual-color deep-tissue three-photon microscopy with a multiband infrared laser. *Light Sci Appl* **2018**, *7*, 12.
8. Qin, Y.; Ou, Y.; Cromey. B.; Batjargal, O.; Barton, J. K.; Kieu, K. Watt-level all- fiber optical parametric chirped-pulse amplifier working at 1300nm. *Opt lett* **2019**, *44*, 3422-3425.
9. Khegai, A. M.; Afanas'ev, F. V.; Riumkin, K. E.; Firstov, S. V.; Khopin, V. F.; Myasnikov, D. V.; Mel'kumov, M. A.; Dianov, E. M. Picosecond 1.3-μm bismuth fibre laser mode-locked by a nonlinear loop mirror. *Quantum Electron* **2016**, *46*, 1077-1081.
10. Thipparapu, N. K.; Guo, C.; Umnikov, A. A.; Barua, P.; Taranta, A.; Sahu, J. K. Bismuth-doped all-fiber mode-locked laser operating at 1340 nm. *Opt Lett* **2017**, *42*, 5102–5105.
11. Khegai, A.; Melkumov, M.; Firstov, S.; Riumkin, K.; Gladush, Y.; Alyshev, S.; Lobanov, A.; Khopin, V.; Afanasiev, F.; Nasibulin, A. G.; Dianov, E. Bismuth-doped fber laser at 1.32 μm mode-locked by single-walled carbon nanotubes. *Opt Express* **2018**, *26*, 23911–23917.
12. Ahmad, H.; Aidit, S. N.; Ooi, S. I.; Samion, M. Z.; Wang, S.; Wang, Y.; Sahu, J. K.; Zamzuri, A. K. 1.3 μm dissipative soliton resonance generation in Bismuth doped fiber laser. *Sci Rep* **2021**, *11*, 6356.
13. Wen, X.; Qiao, T.; Dong, X.; Zhou, M.; Wong, K. K. Bismuth-Doped Fiber Laser at 1.3 μm Mode-Locked By Nonlinear Polarization Rotation. Conference on Lsers and Electro-Optics, Charlotte, NC, USA, 5 May 2024.
14. Chung, H.; Liu, W.; Cao, Q.; Song, L.; Kärtner F. X.; Chang, G. Megawatt peak power tunable femtosecond source based on self-phase modulation enabled spectral selection. *Opt Express* **2018**, *26*, 3684-3695.
15. Takayanagi, J.; Sugiura, T.; Yoshida, M.; Nishizawa, N. 1.0–1.7-m Wavelength-Tunable Ultrashort-Pulse Generation Using Femtosecond Yb-Doped Fiber Laser and Photonic Crystal Fiber. *IEEE Photonics Technol Lett* **2006**, *18*, 2284-2286.
16. Kharenko, D.S.; Efremov, V. D.; Evmenova, E. A.; Babin, S. A. Generation of Raman dissipative solitons near 1.3 microns in a phosphosilicate-fiber cavity. *Opt Express* **2018**, *26*, 15084-15089.

 doi:10.20944/preprints202507.1425.v1

17. Gumenyuk, R.; Puustinen, J.; Shubin, A. V.; Bufetov, I. A.; Dianov, E. M.; Okhotnikov, O. G. 1.32 μm mode-locked bismuth-doped fiber laser operating in anomalous and normal dispersion regimes. *Opt Lett* **2013**, *38*, 4005-4007.
18. Rishøj, L.; Prabhakar, G.; Demas, J.; Ramachandran, S. 30 nJ, ~50 fs All-Fiber Source at 1300 nm using Soliton Shifting in LMA HOM Fiber. Conference on Lasers and Electro-Optics, San Jose, CA, USA, 5 June 2016.
19. Eisenberg, Y.; Wang, W.; Chen, Y.; Antonio-Lopez, J. E.; Amezcua-Correa, R.; Xu, C.; Wise, F. W. Multi-megawatt pulses from 1030 to 1300 nm based on soliton self-frequency shifting in a nitrogen-filled fiber. *Opt Lett* **2025**, *50*, 1593-1596.
20. Russell, P. St. J.; Hölzer, P.; Wang, W.; Abdolvand, Travers, J. C. Hollow-core photonic crystal fibres for gas-based nonlinear optics. *Nat Photonics* **2014**, 8, 278-286.
21. Liang, X.; Fu, L. Enhanced self-phase modulation enables a 700–900 nm linear compressible continuum for multicolor two-photon microscopy. *IEEE J Sel Top Quantum Electron* **2014**, *20*, 42-49.
22. Sidorenko, P.; Fu, W.; Wise, F. Nonlinear ultrafast fiber amplifiers beyond the gain-narrowing limit. *Optica* **2019**, *6*, 1328-1333.
23. Nishizawa, N.; Suga, H.; Yamanaka, M. Investigation of dispersion-managed, polarization-maintaining Er-doped figure-nine ultrashort-pulse fiber laser. *Opt Express* **2019**, *27*, 19218-19232.
24. Schreiber, T.; Ortaç, B.; Limpert, J.; Tünnermann, A. On the study of pulse evolution in ultra-short pulse mode-locked fiber lasers by numerical simulations. *Opt Express* **2007**, *15*, 8252-8262.
25. Hung, H.; Chou, L.; Chan, C.; Wen, C.; Chia, S. Generation of sub-megawatt peak power femtosecond pulses from a 24 MHz Cr:forsterite oscillator. Conference on lasers and Electro-Optics, San Jose, CA, USA, 9 May 2021.